



POLİTEKNİK DERGİSİ

*JOURNAL of POLYTECHNIC*

ISSN: 1302-0900 (PRINT), ISSN: 2147-9429 (ONLINE)

URL: <http://dergipark.gov.tr/politeknik>



## Experimental and Finite Element Methods prediction of 3D printed material mechanical properties with various porosity

*DeneySEL ve sonlu elemanlar yöntemleri 3D baskılı malzemenin çeşitli gözeneklilik ile öngörülmesi*

*Yazar (Author): Abdulaziz S. ALABOODI*

*ORCID: 0000-0003-0370-5324*

**Bu makaleye şu şekilde atıfta bulunabilirsiniz (To cite to this article):** Alaboodi A. S., "Experimental and finite element methods prediction of 3D printed material mechanical properties with various porosity", *Politeknik Dergisi*, 23(1): 121-127, (2020).

**Erişim linki (To link to this article):** <http://dergipark.gov.tr/politeknik/archive>

**DOI:** 10.2339/politeknik.480248

# DeneySEL ve Sonlu Elemanlar Yöntemleri 3D Baskılı Malzemenin Çeşitli Gözeneklilik ile Öngörülmesi

*Araştırma Makalesi / Research Article*

**Abdulaziz S. ALABOODI\***

Department of Mechanical Engineering, College of Engineering, Qassim University, Saudi Arabia

(Geliş/Received : 08.11.2018 ; Kabul/Accepted : 13.03.2019)

## ÖZ

Bu makalede, belirli geometriye sahip modellerin elastik modülü ve akma dayanımı değerlendirilmiştir. Bunun için deneysel ve teorik çalışmalar yapılmıştır. Üretilen modeller, bir pres altında sıkıştırma testine tabi tutulmuş ve ANSYS programında ise analiz (FEA) edilmiştir. Elde edilen sonuçlar, mukavemet, süneklik, ve kilo kaybı açısından en uygun gözeneklilik yüzdesinin belirlenmesinde kullanılmıştır. Sonuçlar n kuvveti, süneklik ve ağırlık azaltmayı koruyan uygun gözeneklilik yüzdesini değerlendirmek için kullanılmıştır. Dayanıklılık, elastik ve plastik modül verimi, porozitenin artmasıyla azalmıştır. En önemli değişiklik elastik modülünde ortaya çıkmıştır.

**Anahtar Kelimeler:** Porozite, 3D yazıcı, sonlu elemanlar analizi.

## Experimental and Finite Element Methods Prediction of 3D Printed Material Mechanical Properties with Various Porosity

### ABSTRACT

In this article, elastic modulus and yield strength of models with specific geometry are evaluated. Experimental and theoretical studies were carried out. Produced models were subjected to compression test under one press and analysis (FEA) in ANSYS program. The results were used to determine the most suitable porosity in terms of strength, ductility, and weight loss. The results were used to assess the percentage of proper porosity that protects the force, ductility and weight reduction. Durability, elastic and plastic module yield decreased with increasing porosity. The most important change occurred in the elastic modulus.

**Keywords:** Porosity, 3D printer, finite element analysis

### 1. INTRODUCTION

Porosity in materials takes different shapes and geometry. It is noticed in biomaterial such as bones and natural material such as sponges, and it could be fabricated as an artificial material. An example of artificial porous material is bone replacement material. The impeded porous structure during bone scaffold fabrication is essential. Several methods have been developed to reach the porous formation in scaffold. These methods include freeze drying, gas forming, phase separation, or solvent casting particulate leaching. These methods are simple and common due to their simplicity; however, they introduce organic solvents to dissolve synthetic polymers which create significant problems. Furthermore, the dimensional control in scaffold specifications such as pore size, pore shape, pore interconnectivity, and pore distribution are the main concerns of these procedures[1].

The most important parameters of porous material such as the size of the pore and the joining were discussed and reported. The deformation of a porous titanium with low

porosity has been investigated via plane strain two dimensional and three-dimensional finite element models[2]. They have simulated the material microstructure of a porous material with 15% porosity. They have concluded that the 3D models of macroscopic response had agreed with the theoretical and experimental results. Although the 3D model's microscopic response had predicted a higher mean of equivalent plastic strain and Von Mises stress than the 2D models. An FEM model has been built corresponding to an open-cell foam solid geometry for simulating the behavior of material in the micro-tension[3]. The steps of modelling start through image analysis, then 3D reconstruction, and then the transformation of the STL file format to solid model imported to the FE package (ANSYS). The shear stress distributions of scaffolds have been investigated using the numerical methods[4]. They have prepared the scaffolds by salt leaching with different geometric specifications. Then the 3D structure obtained using micro-computed tomography. Moreover, they modelled the flow of osteogenic media through the scaffolds by the lattice Boltzmann technique. The fluid flow in single-phase and solute transport have been modeled using FEA and 3D pore geometries which were

\*Sorumlu Yazar (Corresponding Author)  
e-mail : alaboodi@qec.edu.sa

obtained experimentally[5]. Three forms of scaffolds were designed and fabricated via a 3D printing system rapid prototyping technology[6]. An alternative method for investigating and analyzing the mechanical behavior of the structure of bone trabecular have been developed to assist physicians in drug treatment, diagnosis, and monitoring [7]. The bovine bone mechanical properties and three metallic foam materials have been studied using a compression test machine, micro-focus computed tomography, and finite element modelling[8]. The analysis of variance (ANOVA) and finite element methods (FEM) have been presented to investigate the spherical and ellipsoidal voids inside polymer materials[1]. They have found that the initial void, volume fraction, and stress tri-axiality were the most influential parameters. The mechanical behavior characteristics have been evaluated for hydroxyapatite (HA) material induced via bone ingrowth in a rabbit [10]. Their results showed that the internal microstructures influenced the mechanical properties and development of bone regeneration with the time period of implantation. The computational study has been proposed for the mechanical behavior of HA-nanocomposites reinforced with graphene nanosheet and CNT[11]. The effects of void and porosity size have been investigated on effective elastic properties using random fields and finite element 3D models[12]. The parametric optimization technique using the design of experiments have been developed to estimate the 3D printing ability for fabricating scaffold models of calcium sulfate-based[13].

The parameters of 3D printing used in their study were time between two layers, layer thickness, orientation of the product, porosity, mechanical stiffness, and dimensional accuracy by the design of experiments. Honeycomb-like metallic glass (MG) models were fabricated with several relative densities[14]. Their results showed that the 3D-MGs provided high elasticity which was better than ceramics and conventional metals. Numerical and experimental approaches have been used to study the 3D microstructural mechanical performance and failures of 3D printed parts of acrylonitrile butadiene styrene material[15]. They have introduced a structural satisfaction of mechanical criteria up to a certain percentage of porosity. A porous pure Ti samples with different porosities percentage have been fabricated by a laser engineered net shaping method[15]. They have evaluated the mechanical properties of samples using compressive loading. In addition, they have used finite element analysis to study the behavior of the sample's deformation.

The objective of this research was to introduce 3x3x3 cells of porous material that satisfy some conditions. The proposed model could prevent the longitudinal porous cavity by using multidirectional cavities to create obstacles to the crack propagation and to ensure the uniform fluid flow inside the porous cavity material as a web canal. The main objectives of this research are studying the effect of porosity percentage on the mechanical properties of selected material and geometry

using experimental methods. In addition, the effect of porosity percentage on the mechanical properties of selected material and geometry using finite element (FE) method. Then comparing the FEM and experimental results.

## 2. MODELING

The porosity contains three elliptical cylinders oriented on three main directions on the reverse of the Cartesian coordinate. The dimensional parameter was the projection circle radius. By varying the radius, the porosity percentage would change correspondingly. The porosity was the ratio of material of solid volume to the total volume. The proposed model could prevent the longitudinal porous cavity by using multidirectional cavities to create obstacles to the crack propagation and to ensure the uniform fluid flow inside the porous cavity material as a web canal. Some researchers developed porous models with regular and symmetry geometry of porosity. The major benefit of regular porosity geometry modeling is to have variable parameters suitable to be optimized. The porous model should be capable to transmit fluid through the porous material with uniform distribution.

The introduction of porosity would variate its mechanical properties: the elastic modulus, yield strength, and ultimate strength. The 3D matrix model has been developed using a single cell joined together in all the three directions. The matrix configuration (arrangement) between cells is side by side; FE methods would utilize to investigate the cells matrix by introducing a fixed lower side and applying a fixed displacement to the upper side. The direction of displacement is downward that indicates compression load. The applied displacement has been used to overcome the elastic region and to take a portion of the plastic region. Thus, it can estimate the elastic modulus and the yield strength for each set of the cube length by running the model simulation and calculating the maximum strength intensity factor. Further, the model has been used for studying the effect of variation in the single cell parameters and the volume ratio with the maximum strength intensity factor using the side-by-side and mirror matrix configurations. The main objective of this study is to design specific geometry to achieve some properties in the three directional with regular and non-straight porosity channels.

The porosity contains three elliptical cylinders oriented on three main directions in the reverse of the Cartesian coordinates. The dimensional parameter is the projection circle radius. By varying the radius, the porosity percentage will change correspondingly. The fabricated models include a regular shape with certain dimensional parameters. The porosity contains three elliptical cylinders oriented on three main directions in the reverse of the Cartesian coordinate. This model allows any liquid to flow with uniform distribution and transmit through the pore's media. A different configuration with different

orientation of the single model cell would introduce a different collection of models.

**2.1 Material Modeling**

The material used in this paper is metallic plastic [Nylon Plastic filled with Aluminum dust]. It is easy to be used in a 3D printer with good dimensional accuracy. The mechanical properties of the sheet of material delivered from the material provider is not similar to the material produced by 3D printer depending on the printing parameters, adhesive, additive, and other parameters. Thus, it is necessary to take a specimen without porosity to test it and obtain its mechanical properties using a compression test.

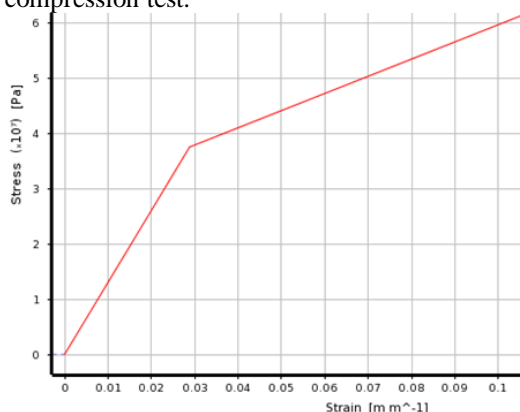


**Figure 1.** Yield Strength Verse Porosity with exponential fit

Figure 1 stress strain curve o the material selected to be investigated. Figure 2 shows the method of predicting the yield strength from the stress strain curve. Similarly, the calculation of yield strength, elastic, and plastic modulus is given below:

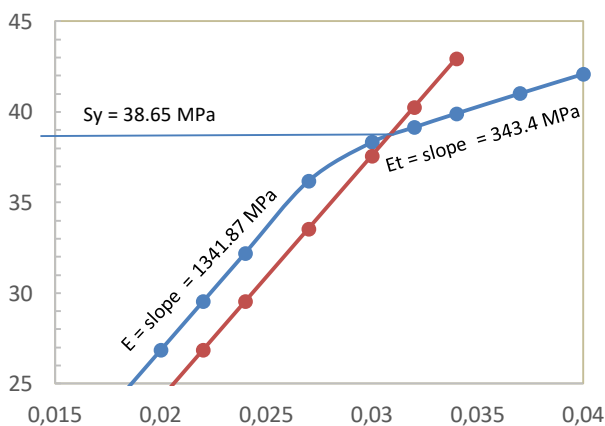


**Figure 2.** Mechanical Properties estimation of bulk material.

The elastic modulus  $E$  (MPa) of each model was defined as in equation (1):

$$E = \frac{\sigma}{\epsilon} = \left(\frac{F}{A}\right) \left(\frac{L}{\Delta L}\right) \quad (1)$$

where  $F$  (N) is the compressive force,  $A$  (mm<sup>2</sup>) is the surface area of load,  $\Delta L$  (mm) the longitudinal deformation, and  $L$ (mm) is the length of the cube.

$$n \frac{L}{A} = constant \quad (2)$$

Where:

$$A = (L)^2 - n (\pi r^2), \text{ for, } n = \text{number of circles.}$$

The amount of deformation  $\Delta L$  was determined as the average axial displacements of all nodes on the loaded surface. In the first step, the pore size of four FE models was increased and the resulting scaffold porosity was calculated according to Eq. 3:

$$Porosity = (1 - Ve/Vo) \times 100\% \quad (3)$$

where  $V_o$  is the overall volume enclosed by the outer periphery and  $V_e$  is the effective volume of the scaffold struts. The effective volume was also evaluated using ANSYS software for each case. The ratio of the solid volume of the material to the total volume should be in the range of 80-90% to mimic the real bon volume ratio. The porosity should be in the range of 10-20%, while in this model extended to be 0-55% to include further range for comparison. The proposed model should prevent the longitudinal porous cavity by using zigzag hollows to create obstacles to the crack propagation and to ensure the uniform fluid flows inside the porous cavity material by using web canals. Here, the 3D matrix was formed by introducing a single cell in all the three direction. The matrix configuration (arrangement) between cells is side by side. For the metallic-plastic with plastic-elastic properties can be characterized by the essential properties using SLM. The Young’s modulus of mean average for metallic-plastic are shown in Table 1. The room temperature was the choice for the model simulation.

**Table 1.** Metallic plastic bulk mechanical properties

Property	Value
Young's Modulus (E) MPa	1301.44
Poisson's Ratio	0.33
Yield Stress MPa	37.50
Plastic Modulus MPa	310.70

**2.2 Geometric Modelling**

The model includes a regular shape with certain dimensional parameters. The porosity contains three elliptical cylinders oriented on three main directions on the reverse of the Cartesian coordinate as in Figure 3. This model allows any liquid to uniform distribution flow and transmit through the bone bourse media. A different configuration with different orientation of the single model cell would introduce a different collection of models.

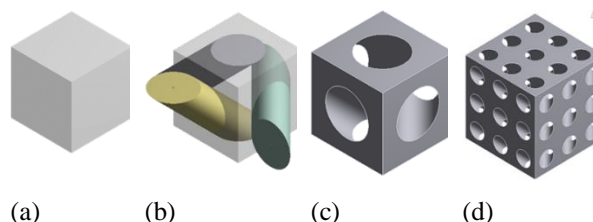


**Figure 3.** Cube (a), with cylindrical cavities (b), subtracted through the six faces (c), 3x3x3 matrix (d)

**2.3 FINITE ELEMENT MODELING**

Finite element methods were also used here to investigate the cells matrix by introducing a fixed lower side and applying a fixed displacement to the upper side as illustrated in Figure 4. The direction of displacement is downward and that indicates compression load. The applied displacement could be used to overcome the elastic region and to take a portion of the plastic region. Thus, we can estimate the elastic modulus and the yield strength for each set of the cube length by running the model simulation and calculating the maximum strength intensity factor. Further, it was aimed here for studying the effect of variation in the single cell parameters and the volume ratio with the maximum strength intensity factor using the side-by-side and mirror matrix configurations.

The process of simulating the compression on the cubic is done through finite element analysis software. All finite element analyzing follows the same steps. The ANSYS Workbench Explicit is used as the FEA (finite element analysis) software. In order to validate the simulation results, the calibration test simulation is done so that the results of the simulation and experiment can be compared. The 3D matrix model has been introducing using single cell joined together to be three cells on three directions. The matrix configuration (arrangement) between cells is side by side. Finite Element methods would be utilized to investigate the cells' matrix by introducing a fixed lower side and applying a fixed displacement to the upper side as illustrated in Figure 4.

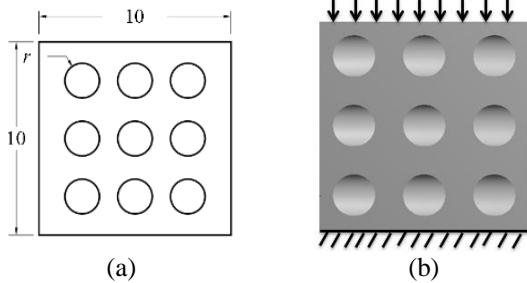


**Figure 4.** 2D views of the 3x3x3 cells Model showing dimension (a), and boundary condition (b).

The exact volume could be attained by extracting the cavities. Then the porosity was calculated. Table 2 shows the side circular radius, circular cross-sectional area, volume, and porosity of each cube.

**Table 2.** Radius of circular cross section area, Volume and porosity of each sample

Radius mm	C.S. Area mm <sup>2</sup>	Volume mm <sup>3</sup>	Porosity %
0	100	1000.0	0.0
2/6	96.86	954.7	4.5
3/6	92.93	898.0	10.2
4/6	87.43	818.7	18.1
5/6	80.36	716.7	28.3
6/6	71.71	592.1	40.8
7/6	61.50	444.8	55.5

The relation between radius and porosity fits exactly as a power equation as shown in Figure 5.

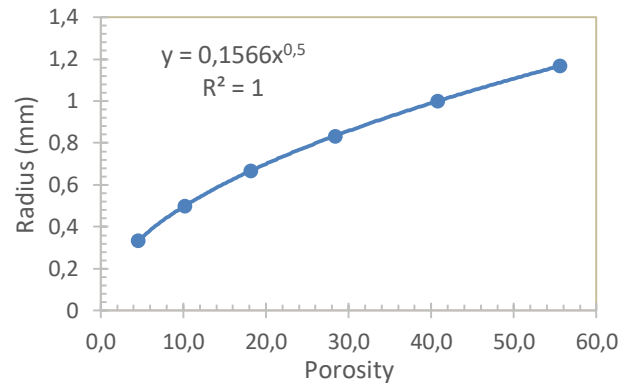


**Figure 5.** Relation between the circle cross sectional radius and porosity %

The direction of displacement is downward, that indicates compression load. The applied displacement will be used to overcome the elastic region and to take a portion of the plastic region. Thus, we can estimate the elastic modulus and the yield strength for each set of the cube length. We can run the model simulation and calculate the maximum strength intensity factor, study the effect of variation of the single cell parameters and the volume ratio with the maximum strength intensity factor using the side-by-side and mirror matrix configurations.

The areas which would receive higher amounts of stress, usually have a higher node density than those which experience little or no stress. The tetrahedron method is used to mesh all the models involved in compression on the cube. The mesh size is given the following characteristics: 0.045 mm minimum edge length, coarse relevance center, high smoothing, and slow transitions. The models are meshed using the appropriate elemental size for the problem examined until a certain mesh size with very small variation results. Figure 6 shows the 3D cubic porous solid model and the mesh of the cube.

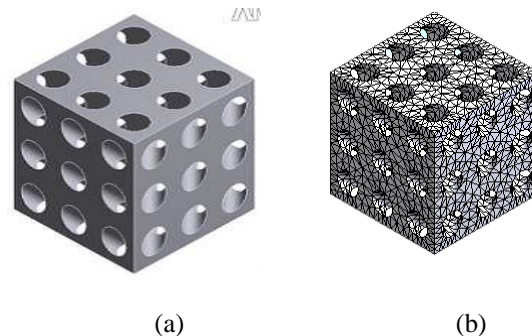


**Figure 6.** 3x3x3 matrix of the single cell to produce (a) 3D cubic porous solid model and (b) mesh of the cube matrix

**3. RESULTS AND DISCUSSION**










Samples were selected for a compression test to investigate the effect of porosity on the mechanical

properties (yield strength, elastic modulus, and plastic modulus). All of the samples were printed via the 3D printer using metallic plastic material as a cube with a 10 mm edge. The first sample was bulk without porosity.

**3.1 Experimental Results**

After preparing the samples with variable porosity (0-55%), the compression test was performed to identify the mechanical properties variation with the variation porosity. Table 3 shows the variation of porosity, 3D CAD model, 3D printed samples, and the sample after deformation.

**Table 3.** Porosity, 3D CAD model, 3D printed samples, and the sample after deformation

Porosity %	3D-CAD Model	Printed sample	After Deformation
0			
18.1			
55.5			

The selected mechanical properties were elastic, plastic modulus and yield strength. Figure 7 illustrated the different stress-strain curves with the variation of porosity using a compression test machine. It was observed that the compressive flow stress-strain curves started to decrease gradually as the porosity of the sample increased up to the sample having a porosity of 10.2 and then it started to decrease drastically beyond the value of porosity of 10.2%. Further, it was observed here that three scaffolds samples having a porosity of 0, 4.5, and 10.2% underwent elastic displacement initially followed by plastic deformation. However, the remaining three samples having a porosity of 28.3%, 40.8%, and 55.5% exhibited little elastic deformation compared to other samples, and these samples were undergoing constant plastic deformation without increasing stress. These results explained that the internally modified sample structures had significantly influenced the mechanical properties of the 3D printed samples. Furthermore, it can be observed that the yield strength, elastic modulus, and plastic modulus started to decrease considerably as the percentage of porosity increased up to 10.2%, and then

these mechanical properties were decreased drastically beyond the 10.2% porosity level in the sample structure. Therefore, it can be concluded here that the samples of 4.5% and 10.2% porosity can be considered for fabrication of implant scaffold bones which has some benefits by the pore's formation in the structures and consequently it can help biologically. Among all the samples investigated here, the 3D printed 4.5% porosity sample can select the optimum one which can be suggested for medical industries.

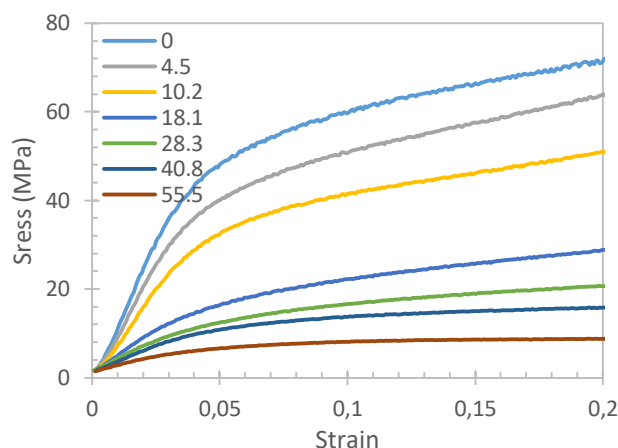


**Figure 7.** Stress-Strain Curves Using Different Porosity (Experimental Results)

**3.2 Finite Element Results**

Using the mechanical properties obtained from experimental results of the bulk cube compression test from table 1, the finite element package (ANSYS) was utilized to simulate the compression test with variable porosity and similar dimensions of the experimental cube. Figure 8 simulated stress strain curves were illustrated using various porosity. It was shown here that for each curve, it showed line with two slopes and an inclination between them. The first slope indicates the elastic modulus and the second slope for plastic modulus and the inclination points indicate the yielding strength.

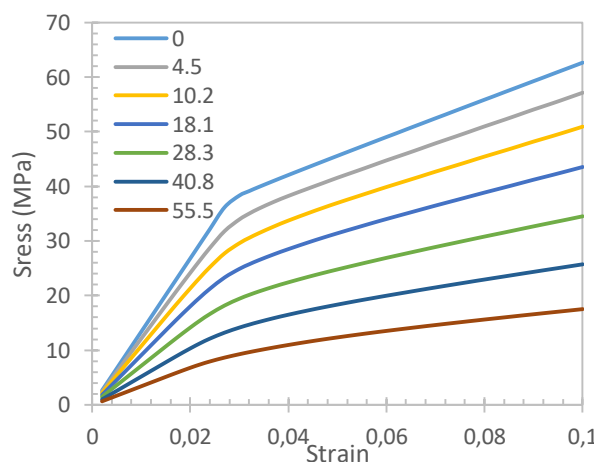


**Figure 8.** Stress-Strain Curves Using Different Porosity (FE Results)

The yield strength versus porosity curve was drawn and the same is shown in Figure 9. The polynomial with the second order fit was used with a good R-square of 0.9981. It showed that the yield strength decreased with an increase in porosity. From zero porosity to 25%, the yield strength was decreased by 18 MPa, whereas it was decreased by only 10 MPa from 25 to 50% of porosity.

At the previous sections, the results of the experimental and finite elements methods were illustrated and described. In this section, the comparison between the two methods results will be introduced. Using the second order polynomial fit, the results of the two methods were drawn in Figure 10. The curves converge at the ends while it diverges at the middle. The maximum variance between the two methods is around the porosity of 25%, which is a reach of about 10 MPa. Similar behavior on the elastic modulus results in Figure 11 and plastic modulus results with errors of 400 MPa and 100 MPa respectively at 35% porosity of both.

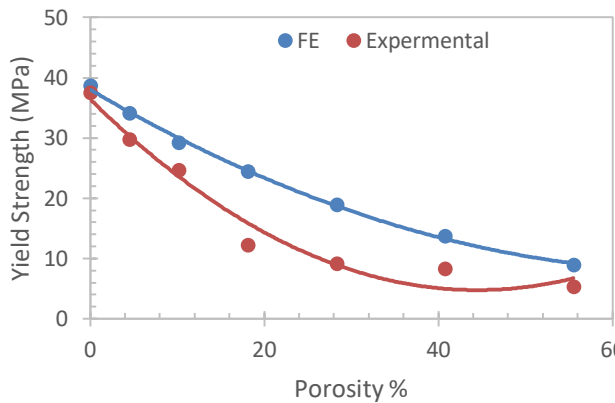


Figure 9. Yield Strength vs Porosity % (FE and Experimental Results)

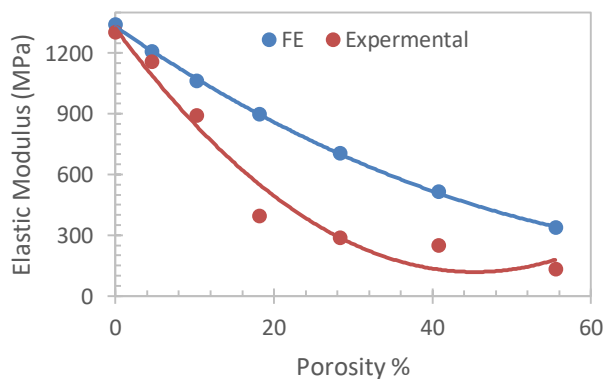


Figure 10. Elastic Modulus vs Porosity % (FE and Experimental Results)

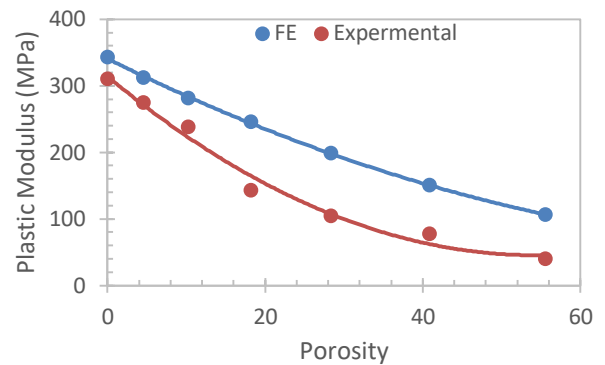


Figure 11. Plastic Modulus vs Porosity % (FE and Experimental Results)

The experimental and finite element results have shown a similar trend with a good polynomial second order fit. The two methods showed agreements at and near the end of the two curves while it diverge at the middle. The reasons of error are that there are many parameters controlling the experimental results such as printing parameters, conditions of materials and adhesive materials, temperature and grains, and grain boundaries with different porosity that were not considered in the finite elements methods. In general, and because of those parameters, the finite elements methods showed results with higher values than the experimental results.

#### 4. CONCLUSION

A simple and effective representation of geometry for regular porous material modelling was proposed using experimental and finite element simulation to investigate the porosity in material and its mechanical properties. Compression load was applied to the top surface of the model using gradual displacement downward from the y-axis. The lower surface was fixed from any movement. Displacement range was chosen to guarantee the model which accomplished full elastic region and portion of the plastic region. The yield strength, elastic, and plastic modulus was evaluated with the variation of the porosity using the same geometry. The experimental and finite elements results show a small variation. The variation increased on the medium range of porosity and decreased for small and large porosity. The most important mechanical property is the yield strength which is decreased with the increase of porosity with approximately half the value.

#### REFERENCES

- [1] Alaboodi, A. S., and S. Sivasankaran. "Experimental design and investigation on the mechanical behavior of novel 3D printed biocompatibility polycarbonate scaffolds for medical applications." *Journal of Manufacturing Processes* 35: 479-491, (2018).

- [2] Shen, H., and L. C. Brinson. "Finite element modeling of porous titanium." *International Journal of Solids and Structures* 44(1): 320-335, (2007).
- [3] N. Michailidis, F. Stergioudi, H. Omar, D. Tsipas, "FEM modeling of the response of porous Al in compression", *Computational Materials Science* 48: 282–286, (2010).
- [4] Roman Voronov, Samuel VanGordon, Vassilios I. Sikavitsas, Dimitrios V. Papavassiliou, "Computational modeling of flow-induced shear stresses within 3D salt-leached porous scaffolds imaged via micro-CT", *Journal of Biomechanics* 43: 1279–1286, (2010).
- [5] Yan Zaretskiy, Sebastian Geiger, Ken Sorbie, Malte Förster, "Efficient flow and transport simulations in reconstructed 3D pore geometries", *Advances in Water Resources* 33: 1508–1516, (2010).
- [6] Su A Park, Su Hee Lee, Wan Doo Kim, "Fabrication of porous polycaprolactone/ hydroxyapatite (PCL/HA) blend scaffolds using a 3D plotting system for bone tissue engineering", *Bioprocess Biosyst Eng*, 34: 505–513, (2011).
- [7] L. Podshivalov, A. F.-Y., "3D hierarchical geometric modeling and multiscale FE analysis as a base for individualized medical diagnosis of bone structure", *Bone* 48: 693–703, (2011).
- [8] T. Guillén, Q.-H. Z.-J., "Compressive behaviour of bovine cancellous bone and bone analogous materials, microCT characterisation and FE analysis", *Journal of the Mechanical Behaviour of Biomedical Materials*, 4: 1452–1461, (2011).
- [9] Andrea Spaggiari, Noel O’Dowd, "The influence of void morphology and loading conditions on deformation and failure of porous polymers: A combined finite-element and analysis of variance study", *Computational Materials Science* 64: 41–46, (2012).
- [10] Li-Mei Ren, M. T. "A comparative biomechanical study of bone ingrowth in two porous hydroxyapatite bioceramics", *Applied Surface Science*, 262: 81-88, (2012).
- [11] Kristopher Doll, Ani Ural, "Mechanical Evaluation of Hydroxyapatite Nanocomposites Using Finite Element Modeling", *Journal of Engineering Materials and Technology*, 135: 011007-1, (2013).
- [12] Jumpol Paiboon, D.V. Griffiths, Jinsong Huang, Gordon A. Fenton, "Numerical analysis of effective elastic properties of geomaterials containing voids using 3D random fields and finite elements", *International Journal of Solids and Structures* 50, 3233–3241, (2013).
- [13] Mitra Asadi-Eydivand, Mehran Solati-Hashjin, Arghavan Farzad, Noor Azuan Abu Osman, "Effect of technical parameters on porous structure and strength of 3D printed calcium sulfate prototypes", *Robotics and Computer-Integrated Manufacturing* 37: 57–67, (2016).
- [14] Ze Liu, Wen Chen, Josephine Carstensen, Jittisa Ketkaew, Rodrigo Miguel Ojeda Mota, James K. Guest, Jan Schroers, "3D metallic glass cellular structures", *Acta Materialia* 105: 35e43, (2016).
- [15] O. B. Hassana, S. Guessasma, S. Belhabib, and H. Nouri, "Explaining the Difference Between Real Part and Virtual Design of 3D Printed Porous Polymer at the Microstructural Level", *Macromol. Mater. Eng.*, 301: 566–576, (2016).
- [16] Sandipan Roy, Niloy Khutia, Debdulal Das, Mitun Das, Vamsi Krishna Balla, Amit Bandyopadhyay, Amit Roy Chowdhury, "Understanding compressive deformation behaviour of porous Ti using finite element analysis", *Materials Science and Engineering C*, 64: 436–443, (2016)